Acta Biomaterialia 131 (2021) 472–482

Contents lists available at ScienceDirect

Acta Biomaterialia

journal homepage: www.elsevier.com/locate/actbio

Full length article

Multifunctional antibody-conjugated coiled-coil protein nanoparticles for selective cell targeting

Marcos Gil-Garcia, Salvador Ventura*

Institut de Biotecnologia i de Biomedicina and Departament de Bioquímica i Biologia Molecular, Universitat Autònoma de Barcelona, Bellaterra, Barcelona 08193, Spain

ARTICLE INFO

Article history:
Received 21 February 2021
Revised 20 June 2021
Accepted 23 June 2021
Available online 27 June 2021

Keywords:
Functional inclusion bodies
Coiled-coil
Protein nanoparticles
Antibody
Cell targeting

ABSTRACT

Nanostructures decorated with antibodies (Abs) are applied in bioimaging and therapeutics. However, most covalent conjugation strategies affect Abs functionality. In this study, we aimed to create protein-based nanoparticles to which intact Abs can be attached through tight, specific, and noncovalent interactions. Initially considered waste products, bacterial inclusion bodies (IBs) have been used in biotechnology and biomedicine. However, the amyloid-like nature of IBs limits their functionality and raises safety concerns. To bypass these obstacles, we have recently developed highly functional α-helix-rich IBs exploiting the natural self-assembly capacity of coiled-coil domains. We used this approach to create spherical, submicrometric, biocompatible and fluorescent protein nanoparticles capable of capturing Abs with high affinity. We showed that these IBs can be exploited for Ab-directed cell targeting. Simultaneous decoration of the nanoparticles with two different Abs in a controllable ratio enabled the construction of a bispecific antibody mimic that redirected T lymphocytes specifically to cancer cells. Overall, we describe an easy and cost-effective strategy to produce multivalent, traceable protein nanostructures with the potential to be used for biomedical applications.

Statement of significance

Functional inclusion bodies (IBs) are promising platforms for biomedical and biotechnological applications. These nanoparticles are usually sustained by amyloid-like interactions, which imposes some limitations on their use. In this work, we exploit the natural coiled-coil self-assembly properties to create highly functional, nonamyloid, and fluorescent IBs capable of capturing antibodies. These protein-based nanoparticles are successfully used to specifically and simultaneously target two unrelated cell types and bring them close together, becoming a technology with potential application in bioimaging and immunotherapy.

1. Introduction

The use of microorganisms as cell factories to produce recombinant proteins often leads to the formation of protein inclusion bodies (IBs) in the cytoplasm [1,2]. The formation of such protein-based nanoclusters is the consequence of an inside-the-cell assembly reaction consisting in the establishment of noncovalent intermolecular interactions between different copies of the recombinant protein (Fig. S1). For decades, these refractile aggregates have been considered waste products [3]. However, it has gradually been revealed that IBs might contain a significant degree of properly folded and functional proteins [4,5]. These nanometric protein particles are mechanically stable [6,7] and their production and purification are cost-effective and fully scalable, making them attractive and ready-to-use functional nanostructured materials [8–10]. In this regard, IBs are increasingly used in biotechnological and biomedical applications, i. e., as reusable biocatalysts [11–13] or in cancer therapy, since they can penetrate cells and release antitumoral polypeptides [14,15].

* Corresponding author.
E-mail addresses: marcos.gil.garcia@uab.cat (M. Gil-Garcia), salvador.ventura@uab.cat (S. Ventura).

https://doi.org/10.1016/j.actbio.2021.06.040

The mechanical stability of IBs relies on the amyloid-like nature of the interactions that stabilize these nanoparticles [16–18]. This amyloidogenic character raises two critical concerns. First, the formation of nonnative intermolecular β-sheet conformations comes at the expense of the native structure, implying that a significant fraction of the protein inside IBs becomes necessarily inactivated [18]. Second, together with the release of adequately folded moieties, the liberation of toxic oligomeric β-sheet species from these nanostructures cannot be disregarded. To offer an alternative to classical amyloid-like IBs, we have recently developed functional IBs exploiting the antiparallel coiled-coil fold of the ZapB protein. This domain promotes intracellular self-assembly into nonamyloid, nontoxic, α-helix-rich IBs. The native-like nature of the interactions that sustain these IBs may preclude the inactivation of ZapB-fused globular domains during the assembly reaction, resulting in highly active nanometric particles [19]. This high functionality seems to be a common property of coiled-coil stabilized IBs [11,13,20–22]. Active ZapB-based IBs can be produced in high yields and easily purified to homogeneity [19], thus they are amenable for use in preparative applications.

The globular nature of proteins confers the main advantage onto protein-based materials, allowing the alteration of material functionality by genetic redesign to fit the intended application [23]. We explored the potential of ZapB-based protein nanoparticles to generate functionalized nanostructures by creating a tripartite fusion protein consisting of ZapB, as the assembling unit, sequentially connected to the green fluorescent protein (GFP) and the Z-domain, as the active moieties (ZapB-GFP-Z). GFP is widely used for *in vivo* imaging [24], whereas the Z-domain [25] is an engineered analog of the B-domain of *Staphylococcus aureus* protein A with high affinity (in the nanomolar range) for IgGs [26–28]. The binding of this allα–helix protein to the Fc region of an IgG is mainly mediated by hydrophobic and noncovalent interactions involving residues located at helices 1 and 2 (Fig. S2) [29,30]. Considering this, the objective was to create traceable fluorescent submicrometric particles that can be easily decorated with an antibody of interest and directed to a specific cellular antigen.

Bispecific antibodies (BsAbs) are mAbs engineered to recognize and bind to two different epitopes simultaneously. BsAbs are increasingly used in cancer therapy since they can recognize targets in cancer cells and immune cells, helping to bring the two cell types together and facilitating tumor cell destruction [31–33]. However, the generalized use of these BsAbs in the clinic is hindered by the high costs and low yields of production and the short half-life of these molecules *in vivo* [34]. Dual-targeting nanoparticles conjugated to two different monoclonal antibodies (mAbs) [35] or binding proteins [36] are being developed to bypass these obstacles and generate new therapeutic applications. We show how ZapB-GFP-Z IBs behave as spherical and fluorescent protein nanoparticles that, when decorated with two different antibodies, promote selective interactions between different cell types, specifically redirecting T lymphocytes to tumoral cells.

2. Materials and methods

2.1. Protein production and purification

The ZapB-GFP-Z gene fragment (the DNA sequence is presented in the Supplementary Information) was cloned into a pET-28a vector between the NcoI and BamHI restriction sites.

For the production of ZapB-GFP and ZapB-GFP-Z IBs, *Escherichia coli* (*E. coli*) BL21 (DE3) (Invitrogen, USA) competent cells were transformed with the corresponding plasmids and grown aerobically in Luria-Bertani broth (LB) medium supplemented with 100 μg/mL ampicillin and 50 μg/mL kanamycin, respectively. After absorbance OD_{600} of 0.6 was reached, protein expression was induced by treatment with 1 mM isopropyl β-D-1-thiogalactopyranoside (IPTG) for 6 h at 30 °C. The cells were collected after centrifugation at 5000 g for 20 min and the pelleted cells were resuspended in 400 μL of buffer A (50 mM Tris and 100 mM NaCl, pH 7.4) supplemented with 4 μL of 100 mM PMSF and 6 μL of 10 mg/mL lysozyme. Then, the cells were incubated for 1 h at 37 °C, cooled on ice and sonicated for 3 min at 15% amplitude in 1 s cycles. 4 μL of Nonidet P40 (NP-40) was added to the sonicated cells, and the mixture was incubated for 1 h at 4 °C. Next, 12 μL of 1 M $MgSO_4$ and 10 μL of 1 mg/mL DNase I were added and the mixture was incubated for 45 min at 37 °C. The mixture was centrifuged at 15,000 g for 15 min at 4 °C, and the pellet was washed with buffer A containing 0.5% Triton X-100. All incubations were performed under agitation. Purified IBs were washed three times with buffer A, and the remaining detergent was removed. The purity of the IBs was confirmed by SDS-PAGE, and the protein concentration was estimated by measuring the absorbance of IBs dissolved in guanidine hydrochloride at 280 nm using a Specord 200 Plus spectrophotometer (Analytik Jena, Germany).

For the production of soluble and His-tagged Z-domain, *E. coli* BL21 (DE3) (Invitrogen, USA) competent cells were transformed with the corresponding plasmid and grown aerobically in LB medium supplemented with 50 μg/mL kanamycin. After an absorbance OD_{600} of 0.6 was reached, protein expression was induced by treatment with 1 mM IPTG for 16 h at 20 °C. The cells were collected after centrifugation at 5000 g for 20 min and resuspended in buffer A containing 20 mM imidazole and 1 mM PMSF. The solution was sonicated on ice, and the supernatant was collected after centrifugation at 15,000 g for 30 min, and the protein was purified by a 5 mL HisTrap FF column (GE Healthcare, USA) using an ÄKTA chromatograph (GE Healthcare, USA).

α-Synuclein was produced, purified and aggregated as previously described in Pujols et al. [37].

2.2. Cell fractionation

The distribution of the expressed ZapB-GFP-Z protein in *E. coli* was analyzed by SDS-PAGE. After protein expression, the cells were centrifuged at 5000 g for 20 min and resuspended in buffer A. Then, the cells were lysed by sonication and centrifuged at 15,000 g for 15 min at 4 °C, and the soluble fraction (supernatant) was separated from the insoluble fraction (pellet). The insoluble fraction was resuspended in buffer A to be the same volume as the soluble fraction, and both fractions were heated for 10 min at 98 °C. Finally, 10 μL of the different fractions were loaded onto SDS-PAGE gels.

2.3. Preparation of antibody-loaded IBs

For the preparation of the IgG-IB complexes, 5 μM ZapB-GFP-Z and 5 μM ZapB-GFP IBs were incubated in the presence of 1 μg of IgG for 45 min at room temperature. Due to the nature of the noncovalent but strong interaction between the Z-domain and the IgGs, the preparation of antibody-decorated IBs was performed by simple mixing. Then, the IBs were harvested by centrifugation at 15,000 g for 20 min and resuspended in buffer A. Next, five washing steps were performed to remove unbound antibody molecules and prevent nonspecific binding.

For the competition assay with ZapB-GFP-Z IBs and soluble Z-domain protein, 1 μg of IgG labeled with Alexa Fluor 555 was incubated in the presence of 5 μM ZapB-GFP-Z IBs, either with an excess (50 μM) or without soluble Z-domain. After incubation for 45 min at room temperature, the samples were centrifuged, and the presence of the IgGs labeled with Alexa Fluor 555 in the insoluble fraction (corresponding to the IBs) was analyzed by measuring

their fluorescence in a Jasco FP-8200 fluorescence spectrofluorometer (Jasco Corporation, Japan).

For the determination of the antibody-binding capacity of the ZapB-GFP-Z IBs, 0.5 μg of IgG labeled with Alexa Fluor 555 was incubated in the presence of increasing concentrations of ZapB-GFP-Z IBs (from 0.5 to 20 μM) for 45 min. Then, the GFP and Alexa Fluor 555 fluorescence of the IBs was measured using a Jasco FP-8200 fluorescence spectrofluorometer (Jasco Corporation, Japan).

2.4. Stability in bovine serum

ZapB-GFP-Z IBs were incubated in bovine serum at room temperature for 15 days. Then, samples obtained at different time points were loaded onto SDS-PAGE gels to evaluate the integrity of the ZapB-GFP-Z protein fusion.

2.5. Epifluorescence microscopy

Ten microliters of 5 μM decorated IBs in buffer A were deposited on top of microscopy glass slides and covered with coverslips. Fluorescence was observed using an Eclipse Ts2R-FL inverted microscope (Nikon, Japan) with a C-LED385 filter for eFluor 450 fluorescence (excitation (390/38 nm) and emission (475/90 nm)), C-LED470 filter for GFP fluorescence (excitation (470/40 nm) and emission (534/55 nm)) and C-LED525 filter for Alexa Fluor 555 fluorescence (excitation (525/50 nm) and emission (597/58 nm)).

2.6. Confocal microscopy

Ten microliters of the solution containing 5 μM ZapB-GFP-Z IBs decorated with two different IgGs labeled with eFluor 450 and Alexa Fluor 555 were deposited on top of microscopy glass slides and covered with coverslips. Then, the fluorescence intensity of the different fluorophores (eFluor 450, GFP and Alexa Fluor 555) was observed upon excitation at a specific wavelength for each fluorophore in a Leica SP5 confocal fluorescence microscope (Leica Microsystems, Germany). Undecorated ZapB-GFP-Z IBs at a concentration of 5 μM were used as negative controls, as no fluorescence signal corresponding to eFluor 450 or Alexa Fluor 555 fluorophores was observed.

2.7. Fourier transform infrared spectroscopy (FTIR)

ZapB-GFP-Z IBs at 5 μM were washed with H_2O to remove the presence of salts, placed on ATR crystals and dried under N_2 flow. The experiment was carried out in a Bruker Tensor 27 FTIR (Bruker Optics, USA) supplied with a Specac Golden Gate MKII ATR accessory. The spectrum consisted of 32 acquisitions measured at a resolution of 1 cm^{-1}. The data were acquired and normalized using OPUS MIR Tensor 27 software (Bruker Optics, USA). The IR spectrum was fitted employing the nonlinear peak-fitting equation in PeakFit package v4.12 (Systat Software, USA). The area for each Gaussian curve was calculated in the amide I region from 1700 to 1600 cm^{-1} using the second derivative deconvolution method with PeakFit package v4.12 (Systat Software, USA).

2.8. Circular dichroism (CD) spectroscopy

CD spectroscopy was used to analyze the secondary structure content of the ZapB-GFP-Z IBs. Specifically, 5 μM ZapB-GFP-Z IBs were resuspended in buffer A, and the far-UV CD spectrum was recorded at a 1 nm bandwidth, scan speed of 100 nm/min and response time of 1 s using a Jasco-815 spectropolarimeter (Jasco Corporation, Japan) at 25 °C.

2.9. Scanning electron microscopy (SEM) and dynamic light scattering (DLS)

Scanning electron microscopy (SEM) was used to analyze the morphology of the undecorated and antibody-decorated ZapB-GFP-Z IBs. Specifically, 10 μL of 5 μM IBs with and without antibodies resuspended in H_2O were deposited on silicon wafers (Ted Pella Inc., USA), air-dried and observed using a Merlin scanning electron microscope (Zeiss Merlin, Germany) operating at 2 kV.

Dynamic light scattering (DLS) was used for quantitative size determination of 5 μM ZapB-GFP-Z IBs undecorated or decorated with antibodies. For the determination of the stability of the ZapB-GFP-Z IBs, the size of the nanoparticles was monitored for 15 days. The size of the IBs was determined using a Zetasizer Nano S90 (Malvern Instruments Limited, UK) at 25 °C.

2.10. Congo red (CR) binding assay

A Congo red (CR) assay was performed to determine the presence of amyloid structures. For the CR assay, 5 μM ZapB-GFP-Z IB was resuspended in buffer A and mixed with CR to a final concentration of 10 μM CR. Aggregated α-synuclein was used as a positive control for protein amyloid aggregation. Optical absorption spectra were recorded in the range from 375 to 700 nm in a Specord 200 Plus spectrophotometer (Analytik Jena, Germany). The spectrum of the protein alone was acquired to subtract protein scattering.

2.11. Fluorescence spectra

The emission spectrum of Alexa Fluor 555 IgG was obtained by recording the emitted fluorescence between 560 and 700 nm using an excitation wavelength of 555 nm.

The emission spectrum of eFluor 450 IgG was obtained by recording the emitted fluorescence between 440 and 660 nm using an excitation wavelength of 410 nm.

The emission spectrum of the ZapB-GFP-Z IBs in buffer A was obtained by recording the emitted fluorescence between 500 and 600 nm. The excitation spectrum was obtained by exciting the samples at a range of 400–500 nm.

Three spectra were accumulated at 25 °C using a Jasco FP-8200 fluorescence spectrofluorometer (Jasco Corporation, Japan) with slit widths of 5 nm, a 0.5 nm interval, and a 1000 nm/min scan rate for each sample.

For the thermal unfolding of unloaded and IgG-loaded ZapB-GFP-Z IBs, the GFP fluorescence signal was recorded in a range of 25–95 °C with an increasing heat rate of 1 °C/min and slit widths of 5 nm and 600 rpm. ZapB-GFP-Z IBs were excited at 495 nm and emission was recorded at 514 nm using a Jasco FP-8200 fluorescence spectrofluorometer (Jasco Corporation, Japan).

2.12. Toxicity assay

HeLa cells and MRC-5 cells were seeded into 96-well plates and cultured for 24 h in Dulbecco's Modified Eagle Medium (DMEM) and Minimum Essential Medium α (MEM α), respectively, supplemented with 10% Fetal Bovine Serum (FBS). The ZapB-GFP-Z IBs were resuspended in PBS at pH 7.4 and added at a concentration ranging from 2 to 12 μM. PBS was used alone as a control.

For the evaluation of the potential antibody-associated ZapB-GFP-Z IBs toxicity, HeLa cells were seeded into 96-well plates and cultured in DMEM supplemented with 10% FBS for 24 h. ZapB-GFP-Z IBs loaded with anti-EGFR IgGs were resuspended in PBS at pH 7.4 and added at a concentration ranging from 2 to 12 μM. PBS alone and anti-EGFR IgGs were used as controls.

In the case of the potential toxicity induced by ZapB-GFP-Z IBs loaded with anti-CD3 IgGs, T cells (Jurkat cell line) were seeded

into 96-well plates cultured in Roswell Park Memorial Institute (RPMI) 1640 + GlutaMAX medium supplemented with 10% FBS for 24 h. ZapB-GFP-Z IBs decorated with anti-CD3 IgGs were resuspended in PBS at pH 7.4 and added at a concentration ranging from 2 to 12 μM. PBS alone, anti-CD3 IgGs and undecorated ZapB-GFP-Z IBs at 10 μM were used as controls.

Treated and control cells were incubated at 37 °C in 5% CO_2 for 72 h. Then, 10 μL of PrestoBlue cell viability reagent (Thermo Fisher Scientific) was added and incubated for 30 min. Cell viability was determined by quantifying the fluorescence with a Victor3 fluorescent plate reader (Perkin Elmer, USA).

2.13. Statistical methods

All experimental values are presented as the means ± standard error of the mean (SEM). Measurements are taken in duplicate. GraphPad Prism software (GraphPad Software, USA) was used to calculate the mean and SEM values.

2.14. Specific cell targeting by decorated IBs

HeLa cells were cultured on a 35 mm cell culture dish (SARSTEDT AG & Co, Germany) to a confluence of 70–80%. The initial DMEM was replaced with fresh medium containing 10 μM ZapB-GFP-Z-anti-EGFR IgG IB labeled with Alexa Fluor 555 and prepared as previously described in the "Preparation of antibody-loaded IBs" section. Then, HeLa cells were incubated with ZapB-GFP-Z-anti-EGFR IgG IBs for 1 h at 37 °C and 5% CO_2, and ZapB-GFP-Z-IgG anti-rabbit IBs were used as controls. The incubated cells were washed five times with fresh medium to remove unbound molecules.

T cells were maintained in RPMI 1640 + GlutaMAX medium supplemented with 10% FBS. T cells were harvested and resuspended in fresh medium containing 5 μM ZapB-GFP-Z-anti-CD3 IgG IB labeled with eFluor 450. The cells were incubated with ZapB-GFP-Z-anti-CD3 IgG IBs for 1 h at 37 °C and 5% CO_2, precipitated and washed five times with fresh medium. ZapB-GFP-Z-IgG anti-rabbit and anti-EGFR IBs were used as controls.

For the binding of unrelated cell types, HeLa cells were cultured on a 35 mm dish cell culture (SARSTEDT AG & Co, Germany) to a confluence of 70–80%. Then, the initial medium was replaced with T cells and dual antibody-decorated 10 μM ZapB-GFP-Z IBs (anti-EGFR labeled with Alexa Fluor 555 and anti-CD3 labeled with eFluor 450). The cells with antibody-decorated IBs were incubated for 1 h at 37 °C and 5% CO_2 and washed five times with fresh medium. IBs decorated with only anti-EGFR IgGs were used as controls.

Finally, the cells incubated with decorated IBs were visualized using an Eclipse Ts2R-FL inverted microscope (Nikon, Japan), and images were acquired using the appropriate filters and brightfield.

2.15. Flow cytometry assay

ZapB-GFP-Z IBs were decorated with anti-EGFR IgG labeled with Alexa Fluor 555 as previously described. Then, HeLa cells were incubated with the decorated IBs for 1 h, pelleted and washed five times to discard unbound molecules. HeLa cells incubated with ZapB-GFP IBs (previously incubated with anti-EGFR IgGs), ZapB-GFP-Z IBs decorated with anti-rabbit IgG, ZapB-GFP-Z IBs alone, and buffer alone were used as controls. For the T cell experiments, the procedure was the same as previously described for HeLa cells, decorating ZapB-GFP-Z IBs with anti-CD3 IgG. In this case, T cells incubated with ZapB-GFP IBs (previously incubated with anti-CD3 IgGs), ZapB-GFP-Z IBs decorated with anti-rabbit IgG, ZapB-GFP-Z IBs alone, and buffer alone were used as controls.

A total of 10,000 cells incubated with IBs were analyzed using a FACSCanto flow cytometer (BD Biosciences, USA) equipped with a FITC laser to detect the green fluorescence of GFP. Fluorescence intensities of cell-bound IBs were analyzed and quantified using FlowJo (BD Biosciences, USA).

For the evaluation of the localization of HeLa and T cells in the presence of dual-decorated (anti-EGFR and anti-CD3 IgGs) ZapB-GFP-Z IBs, HeLa cells were cultured on a 35 mm cell culture dish (SARSTEDT AG & Co, Germany) to a confluence of 70–80%. Then, the initial medium was replaced with T cells and dual antibody-decorated 10 μM ZapB-GFP-Z IBs (anti-EGFR and anti-CD3 IgG). Cells with decorated IBs were incubated for 1 h at 37 °C and 5% CO_2 and washed five times with fresh medium. ZapB-GFP-Z IBs decorated with only anti-EGFR IgGs were used as controls. Then, trypsin was added to the solution and neutralized with FBS-supplemented medium. Then, the cells were centrifuged, resuspended in PBS at pH 7.4 and analyzed using a FACSCanto flow cytometer (BD Biosciences, USA). FSC and SSC signals were measured for the detection of both cell types, and untreated HeLa and T cells were used alone as controls. Finally, the percentage and quantification of the cells were determined using FlowJo (BD Biosciences, USA).

3. Results

3.1. ZapB-GFP-Z forms nonamyloid α-helix-rich IBs

To generate nonamyloid fluorescent IBs with antibody capturing activity, ZapB was N-terminally fused to two consecutive globular domains: GFP and the Z-domain. This created a tripartite fusion protein named ZapB-GFP-Z. The Z-domain [25] is an engineered analog of the B domain of *Staphylococcus aureus* protein A, consists of 58 residues (6.6 kDa), and folds into three α-helices. Therefore, the fusion protein consisted of sequentially ordered coiled-coil, all-β, and all α- domains (Fig. S3).

ZapB-GFP-Z was expressed in *E. coli* and located in the insoluble cell fraction (Fig. S4), from which IBs composed of assembled copies of the fusion protein were purified to homogeneity (Fig. S5) at a yield of 98.5 ± 5.5 mg/L. The secondary structure of the IBs was analyzed using Fourier Transform Infrared Spectroscopy (FTIR). We recorded the infrared spectrum of the ZapB-GFP-Z IBs in the amide I region (1700–1600 cm^{-1}), corresponding to the absorption of the main chain carbonyl group. As shown in Fig. 1A, the primary contributor to the ZapB-GFP-Z IBs spectrum was a signal located at 1654 cm^{-1} (44% of the area), assigned to the α-helix conformation. This outcome is reasonable since the ZapB and Z-domains both consist of α-helices. A second band at 1631 cm^{-1} accounts for 35% of the spectrum area and likely represents the low-frequency coiled-coil signal [38] and the β-sheet signal of the GFP β-barrel. The third band at 1676 cm^{-1} (21% of the area) possibly is attributable to the mixed contribution of structurally different domains at high frequencies. Although the far-UV Circular Dichroism (CD) spectrum of the ZapB-GFP-Z IBs is influenced by the β-barrel structure of GFP, the two main α-helical signals are still evident, with a minimum at 224 nm and an inflection at 210 nm, in good agreement with the FTIR data (Fig. S6) and with the previous secondary structure analysis of ZapB IBs and ZapB-GFP IBs [19]. These results corroborate the native-like secondary structure of the ZapB-GFP-Z polypeptides embedded in these IBs.

Scanning Electron Microscopy (SEM) revealed that the ZapB-GFP-Z IBs were of submicrometric size and displayed a spherical shape (Fig. 1B). Dynamic light scattering (DLS) data revealed a moderately polydisperse size distribution with an average diameter of 560 ± 157 nm (Fig. S7) that remained stable in size for at least 15 days (Fig. S8). This submicrometric size is the result of the high order assembly of multiple copies of the ZapB-GFP-Z fusion protein inside the bacteria, already before their purification. To assess whether ZapB-GFP-Z IBs were stable under close to physiolog-

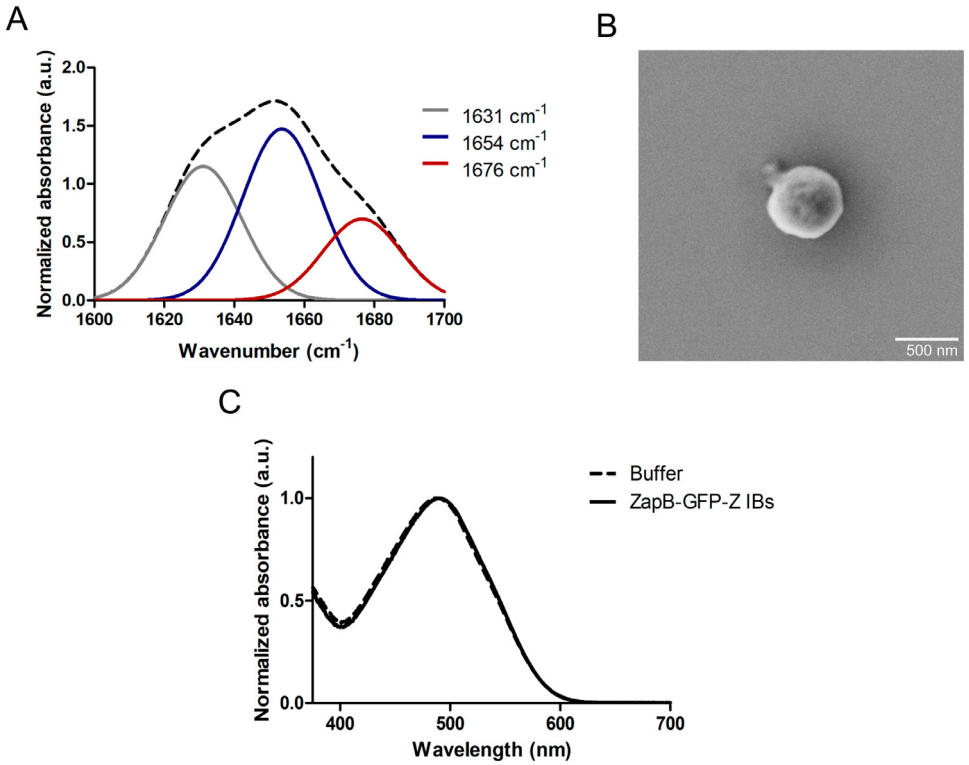

Fig. 1. Conformational properties of the ZapB-GFP-Z IBs. (A) FTIR absorbance spectrum of the ZapB-GFP-Z IBs in the amide I region (dashed line). The different component bands (solid lines) were obtained by deconvolution of the spectrum using PeakFit software. (B) SEM image of a ZapB-GFP-Z IB. (C) CR absorbance spectra of the ZapB-GFP-Z IBs (solid line) and buffer alone (dashed line).

ical conditions, they were incubated with bovine serum for up to 15 days. The SDS-PAGE analysis revealed that the fusion protein in these IBs remained stable for at least 10 days at room temperature (Fig. S9).

An amyloid-like nature for ZapB-GFP-Z IBs was excluded using one of the most common dyes to detect amyloid-like structures, the Congo red (CR) [39]. The CR absorption spectrum is sensitive to the presence of amyloid structures, displaying a redshift in their presence, caused by the cooperative binding of CR molecules along the fibril axis [40]. As shown in Fig. 1C, the spectra of CR dye in the presence and absence of ZapB-GFP-Z IBs were very similar. In contrast, when CR was incubated with aggregated α-synuclein, the displacement of the spectrum was evident (Fig. S10).

Finally, the thermal stability of the fusion protein within the ZapB-GFP-Z IBs was analyzed by monitoring the changes in the GFP fluorescence intensity upon heating. As shown in Fig. S11, the melting curve is indicative of cooperative GFP unfolding with a T_m of 74.5 ± 3.0 °C.

Overall, the biophysical analysis indicates that ZapB-GFP-Z IBs are α-helix-rich and stable nanometric spherical particles, likely sustained by coiled-coil interactions, and devoid of amyloid-like intermolecular β-sheet structures.

3.2. ZapB-GFP-Z IBs are bifunctional

The conformational traits of ZapB-GFP-Z IBs suggest that the different domains in the protein fusion might maintain their native structure in the assembled state. Therefore, they were expected to emit green fluorescence and bind antibodies simultaneously. To confirm that the spectral properties of the GFP embedded in the ZapB-GFP-Z IBs were preserved, the excitation and emission spectra were recorded. As shown in Fig. S12, the GFP located in the IBs displays the characteristic excitation and emission profiles, in good agreement with our previous studies [19], with excitation and emission maxima at 495 nm and 514 nm, respectively. To confirm the expected bifunctional activity of these IBs, we incubated ZapB-GFP-Z IBs with an IgG antibody labeled with Alexa Fluor 555 at room temperature for 45 min. Then, the IBs were precipitated and washed five times to minimize nonspecific binding, and the fluorescence of these nanoparticles was analyzed by fluorescence microscopy. The ZapB-GFP-Z IBs emitted the characteristic GFP green fluorescence and the labeled antibody red fluorescence, with a perfect overlap between both signals (Fig. 2). When ZapB-GFP IBs without the Z-domain were used as controls, green fluorescence was evident, but we could not detect red fluorescence coming from the labeled IgG (Fig. S13), indicating that the Z-domain was essential for the binding of IgG to the IBs. The ability of the ZapB-GFP-Z IBs to bind antibodies was tested in the presence and in the absence of 10-fold molar excess of soluble Z-domain. As shown in Fig. 3A, the binding of these IBs to antibodies labeled with Alexa Fluor 555 was strongly reduced in the presence of the competing soluble Z-domain, as it was evident by the much lower fluorescence intensity. This indicates that, as intended, the binding of the antibodies to the IBs is mediated by the Z-domain.

To determine the IgG loading capacity of these IBs, we performed a titration assay by measuring the fluorescence of the labeled IgG bound to the IBs. As shown in Fig. 3B, the GFP fluorescence of these IBs increases linearly with the concentration. In contrast, the binding of the Alexa Fluor 555-labeled IgG reached a plateau at 2 μM ZapB-GFP-Z IB, revealing a conventional saturation binding curve, with an apparent binding capacity of 130 ng of antibody per μg of IB and 867 ng of antibody per μg of Z-domain in the IB (Fig. 3C).

We characterized the size and morphology of these nanoparticles when loaded with antibodies using DLS and SEM. The pres-

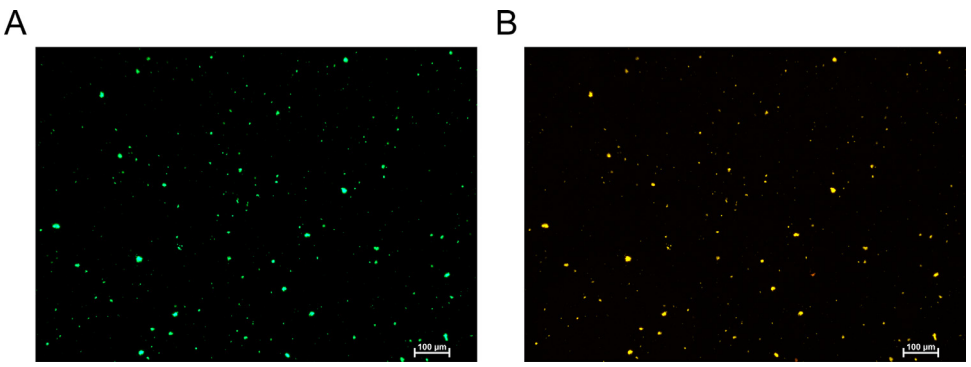

Fig. 2. Bifunctional activity of the ZapB-GFP-Z IBs. Representative fluorescence microscopy images of (A) GFP fluorescence and (B) IgG labeled with Alexa Fluor 555 fluorescence. (For interpretation of the references to color in this figure, the reader is referred to the web version of this article.)

ence of the IgGs increased the average diameter of the IBs to 724.8 ± 292.7 nm, while they kept the spherical shape (Fig. S14). The stability of the IBs constituent fusion proteins was not significantly altered by the presence of the IgGs, as it was deduced from the cooperative melting curve of GFP, with a Tm of 75.0 ± 2.1 °C, fairly similar to that of undecorated IBs (Fig. S11).

3.3. ZapB-GFP-Z IBs are biocompatible

Once the functionality of ZapB-GFP-Z IBs was confirmed, we sought to determine whether they induce toxicity in human cells since it would preclude any further cellular assay. HeLa cells were incubated with different concentrations of ZapB-GFP-Z IBs (from 0 to 12 µM), and we monitored their viability using a PrestoBlue® fluorescent assay. As it can be observed in Fig. 4A, ZapB-GFP-Z IBs did not show associated toxicity at any of the assayed concentrations. The IBs toxicity was further tested in the MRC-5 nontumor human lung fibroblast line. As shown in Fig. 4B, ZapB-GFP-Z IBs were innocuous to MRC-5 cells at all the assayed concentrations, corroborating that these functional protein-based nanoparticles have optimal biocompatibility.

3.4. Antibody-decorated ZapB-GFP-Z IBs specifically target human cancer cells

We aimed to assess whether ZapB-GFP-Z IBs can target specific antigens in living cells once they have been loaded with antibodies through their Z-domain. First, we decorated ZapB-GFP-Z IBs with an anti-EGFR antibody labeled with Alexa Fluor 555 as described above. Anti-EGFR antibodies recognize epidermal growth factor receptor (EGFR) overexpressed on the membrane of epithelial cancer cells such as HeLa cells [41,42]. We incubated the anti-EGFR antibody-loaded ZapB-GFP-Z IBs with HeLa cells. The presence of IBs attached to the cell membranes was corroborated using fluorescence and brightfield microscopy (Fig. 5). We observed a good overlay between green and red fluorescence signals, emitted from the GFP and the antibody, respectively, indicating that the nanoparticles maintained their bifunctionality in the assay. In contrast, when HeLa cells were incubated in the presence of ZapB-GFP-Z IBs loaded with an anti-rabbit antibody, IBs binding to cells was not detected (Fig. S15), indicating that the recognition of HeLa cells by IBs is specific and depends on the presence of anti-EGFR antibodies anchored to their Z-domains.

The binding of IBs to cells was also investigated using flow cytometry (FC). We incubated ZapB-GFP-Z IBs alone and loaded with either anti-EGFR or anti-rabbit antibodies with HeLa cells, followed by a washing step. The cells were immediately analyzed by FC, taking advantage of GFP fluorescence using a FITC emission detector. The analysis revealed that approximately 80% of the HeLa cells were labeled with anti-EGFR decorated IBs (Fig. S16), whereas no significant labeling was observed in the other cases. Similarly, when ZapB-GFP IBs were incubated with the anti-EGFR antibody, and these IBs were added to HeLa cells, the cells remained unlabeled. Furthermore, when ZapB-GFP-Z IBs loaded with anti-EGFR antibody were incubated with cells deficient in EGFR expression, such as T lymphocytes, the IBs did not recognize them (Fig. S17).

Finally, we wanted to discard any antigen-specific toxicity of the antibody-decorated IBs. ZapB-GFP-Z IBs loaded with anti-EGFR antibody were incubated with HeLa cells. As shown in Fig. S18**,** these functionalized IBs did not induce any detectable antigen-associated toxicity in the HeLa cells, which displayed viability values similar to the cells treated with buffer or anti-EGFR soluble antibody.

Overall, we can conclude that ZapB-GFP-Z IBs can be used to target specific human cell epitopes and that this activity depends both on the presence of the Z-domain and the identity of the conjugated antibody, without any antigen-associated toxicity. The intrinsic green fluorescence of these nanoparticles allows to localize them easily without need for post-assembly IBs labeling.

3.5. Dual antibody binding by the ZapB-GFP-Z IBs

In principle, these bifunctional IBs can be endorsed with multivalency simply by loading different IgG antibodies onto the Z-domain. To confirm this possibility, ZapB-GFP-Z IBs were simultaneously incubated with two different antibodies labeled either with Alexa Fluor 555 (red fluorescence) or eFluor 450 (blue fluorescence). As shown in Fig. 6, ZapB-GFP-Z nanoparticles emitted three different fluorescence signals, green from GFP, and red and blue fluorescence from the antibodies, with a perfect overlap, indicating that both antibodies were bound to the IBs, as intended. This dual antibody-loading was confirmed using confocal microscopy. A good overlap of the three fluorescence signals in the dual-decorated IBs was observed, without detecting blue or red fluorescence signals in the undecorated ZapB-GFP-Z IBs (Fig. S19). Moreover, controlling the proportion of the antibodies in the initial mixture allowed us to obtain IBs decorated with a defined ratio of these molecules (Fig. S20).

Overall, the data indicate that ZapB-GFP-Z IBs can be functionalized with the desired proportion of two, and likely more, different antibodies.

3.6. Dual antibody-conjugated ZapB-GFP-Z IBs direct T lymphocytes to HeLa cells

Once we confirmed the ability of ZapB-GFP-Z IBs to capture different antibodies simultaneously, we wondered whether they can be used as scaffolds to bring two different cell types together. To this end, we first analyzed the ability of the ZapB-GFP-Z IBs to tar-

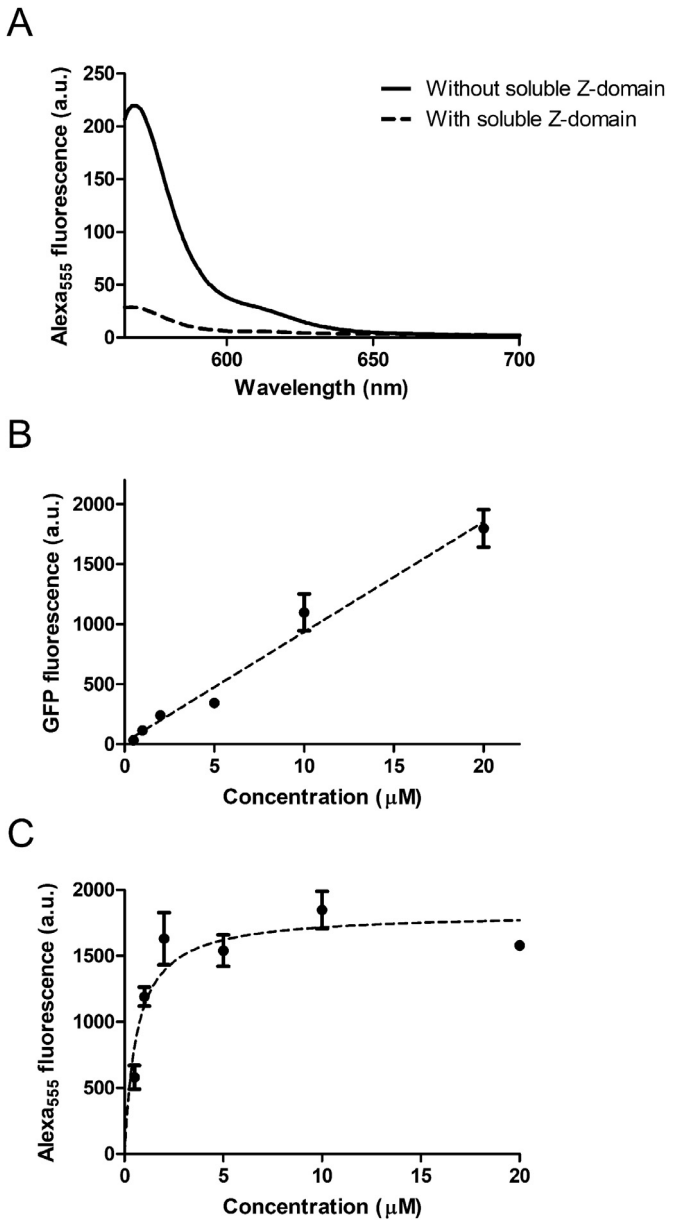

Fig. 3. Antibody-binding capacity of the ZapB-GFP-Z IBs. (A) Alexa Fluor 555 fluorescence intensity of ZapB-GFP-Z IBs incubated with labeled IgG in the presence and absence of excess of competing soluble Z-domain. (B) Fluorescence intensity of GFP of IgG-loaded ZapB-GFP-Z IBs as a function of the IBs concentration. (C) Alexa Fluor 555 fluorescence intensity of IgG-bound to ZapB-GFP-Z IBs as a function of the IBs concentration.

get T lymphocytes when they were decorated with anti-CD3 IgG labeled with eFluor 450. This anti-CD3 antibody recognizes the TCR/CD3 complex of T cells [43]. ZapB-GFP-Z IBs loaded with anti-CD3 IgG were incubated with T cells for one hour and washed to prevent nonspecific binding. As shown in Fig. 7, the presence of conjugated IBs attached to T cells was evident in the fluorescence and brightfield microscopy images. In addition, there was a perfect overlap between the green and blue fluorescence emitted from the GFP and anti-CD3 antibody, respectively. When T cells were incubated with ZapB-GFP-Z IBs loaded with anti-rabbit IgG, these nanoparticles did not recognize the T lymphocytes (Fig. S21).

The binding of IBs to T cells was also investigated using FC, as previously described with HeLa cells. As shown in Fig. S22, the analysis indicated that approximately 60% of T cells were labeled when incubated with ZapB-GFP-Z IBs conjugated to the anti-CD3 antibody. In contrast, T cells incubated with IBs loaded with non-specific antibodies, unloaded IBs or IBs incubated with the anti-CD3 antibody but devoid of the Z-domain remained unlabeled and were nonfluorescent.

To confirm that ZapB-GFP-Z IBs decorated with anti-CD3 antibody did not induce antigen-specific toxicity, T cells were incubated with different concentrations of anti-CD3-loaded IBs for 72 h. As is shown in Fig. S23, these functionalized IBs did not induce any significant toxicity at the tested concentrations.

The data indicate that, as shown for HeLa cells, the binding to T lymphocytes is controlled by the specificity of the bound antibody. Next, we loaded ZapB-GFP-Z IBs simultaneously with two antibodies, namely, fluorescently labeled anti-EGFR and anti-CD3. These dual-antibody decorated IBs were incubated with HeLa and T cells for one hour, and the culture was washed to remove unbound particles. Brightfield microscopy analysis showed abundant circular T cells and polygonal HeLa cells connected by fluorescent IBs (Figs. 8 and S24). In contrast, when HeLa cells and T cells were incubated in the presence of ZapB-GFP-Z IBs loaded only with anti-EGFR IgG, the IBs targeted HeLa cells but did not capture T lymphocytes (Fig. S25).

The IBs mediated colocalization of the two cell types was further studied using FC. As shown in Fig. S26, the dual decoration of ZapB-GFP-Z IBs with anti-EGFR and anti-CD3 antibodies promoted the association of T cells and HeLa cells. However, in the absence of anti-CD3 antibody, the ZapB-GFP-Z IBs failed to promote this cell association. A quantitative analysis indicated that dual anti-EGFR and anti-CD3 antibody decoration of ZapB-GFP-Z IBs increased the number of T cells associated to HeLa cells by at least 14-fold, when compared with IBs decorated only with anti-EGFR antibody (Table S1).

Overall, the data indicate that dual antibody-loaded ZapB-GFP-Z IBs can simultaneously bind at least two different antigens and approach unrelated cell types.

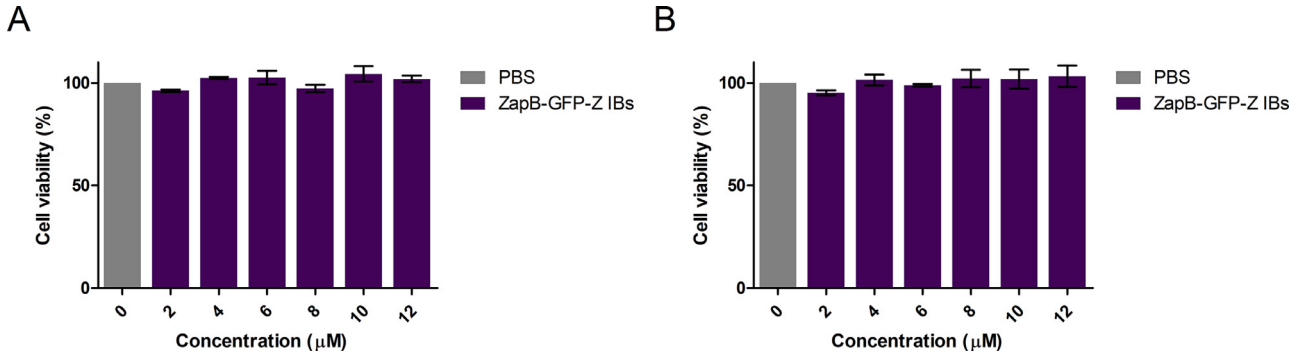

Fig. 4. Cytotoxicity induced by the ZapB-GFP-Z IBs. HeLa (A) and MRC-5 (B) cell viability was tested at different concentrations (from 2 to 12 μM) of ZapB-GFP-Z IBs. IBs were added to the cells and incubated for 72 h. PBS buffer was used as the control.

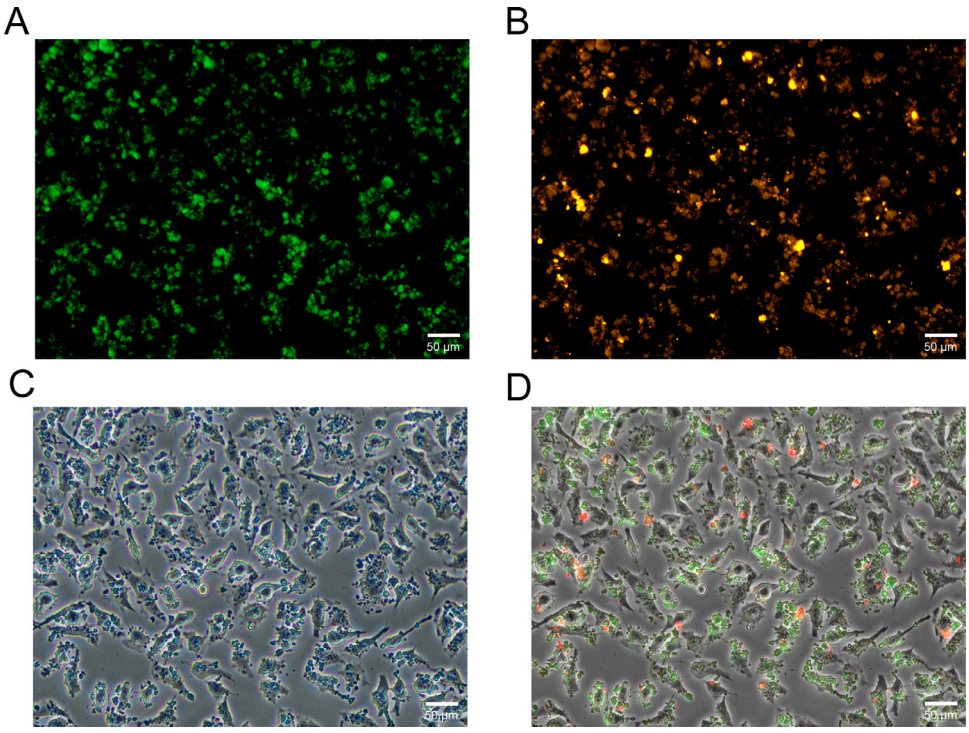

Fig. 5. Specific binding of functionalized ZapB-GFP-Z IBs to human cells. Representative microscopy images of green fluorescence emitted from the ZapB-GFP-Z IBs (A), red fluorescence emitted from anti-EGFR IgG labeled with Alexa Fluor 555 (B), HeLa cells with brightfield microscopy (C), and the three images merged (D). (For interpretation of the references to color in this figure legend, the reader is referred to the web version of this article.)

4. Discussion

Functional IBs are becoming promising sources of active protein for biotechnological and biomedical purposes [44]. These protein nanoparticles are easy to produce and purify at preparative yields and have been applied in tissue engineering, protein delivery, as vaccines, and for catalysis [45–48].

We have recently succeeded in exploiting the ability of a natural coiled-coil domain to self-assemble inside bacterial cells to generate highly active IBs [19]. These α-helix-rich protein nanoparticles overcome the drawbacks of classical β-sheet-rich, amyloid-like IBs. Here, we address whether this inside-the-cell coiled-coil-driven assembly strategy can be used to create multifunctional IBs containing two different folded and active globular domains.

The tripartite ZapB-GFP-Z fusion protein was successfully expressed in *E. coli* cells as IBs. These nanoparticles have been purified to homogeneity, and they display a spherical submicrometric size that remains stable in solution for more than a week, suggesting suitability for their use in nanotechnological or biomedical applications [49,50]. In this study, we showed that these IBs are sustained by native-like α-helical interactions and that the activity of the all-β GFP and all α- Z-domain moieties is preserved, as evidenced by the perfect overlap between the green fluorescence of GFP and the red or blue fluorescence emitted from the labeled IgG antibody attached to the Z-domain. This outcome suggests a generic ability of proteins to keep their active structures within ZapB-based IBs, as indicated by the cooperative melting of the GFP moiety. Importantly, ZapB-GFP-Z IBs keep a submicrometric size when bound to antibodies, without their shape or the constituent proteins stability being altered.

Biomaterials for *in vivo* applications need to be nontoxic to human cells [19]. As intended, generating IBs without amyloid characteristics resulted in innocuous and biocompatible IBs potentially suitable for biomedical purposes, as it has been corroborated with different cell lines. Another requirement for future *in vivo* uses is negligible antigen-specific toxicity when they are loaded with antibodies, a feature that IgG-decorated ZapB-GFP-Z IBs fulfill.

Selective targeting of defined cell types has emerged as a safe alternative to conventional therapies, minimizing toxic side effects. The ability of BsAbs to simultaneously recognize two different epitopes is increasingly exploited in immuno-oncology, gradually displacing monovalent therapies, since this capacity allows redirection of immune cells to selected cancer cell types [51].

Dual-targeting nanoparticles that combine two different mAbs are receiving increasing attention as alternatives to BsAbs for cancer immunotherapy [35]. The FDA has approved many monovalent mAbs for targeted cancer treatment, and these mAbs are manufactured at a much lower cost than BsAbs. In addition, mAb immobilization in a nanoscopic assembly results in significant stabilization relative to short-lived soluble BsAbs. Current methods for developing multivalent antibody nanostructures rely on covalent strategies that require consecutive chemical conjugations steps [52], which can potentially modify the antibody structure and function. In contrast, in ZapB-GFP-Z protein nanoparticles, antibody decoration relies on the strong, specific, and noncovalent interaction between the Z-domain and the Fc-region of IgG, as shown in the competition binding assay, which is not expected to alter the antibody affinity/specificity for its target.

Once we demonstrated the ability of antibody decorated ZapB-GFP-Z IBs to recognize different cell types specifically, we rationalized that our multifunctional nanoparticles can be a convenient way to promote dual epitope targeting when decorated with two different specific antibodies and, indeed, dual-loaded nanoparticles effectively redirect T cells to cancer cells.

The intrinsic fluorescence of these nanostructures makes them traceable *in vivo*, without the need for fluorescent dyes, and they can be simultaneously loaded with two, and likely more, antibodies in a user-defined stoichiometry. These features, together with the high yield of production confer them advantages, relative to BsAbs, from a biotechnological point of view.

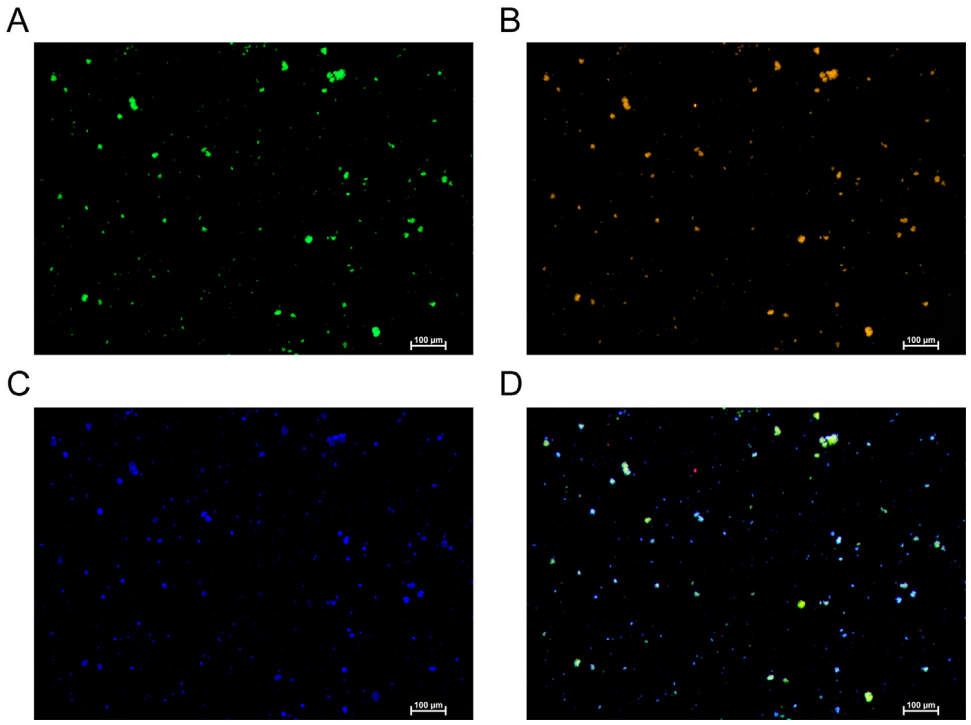

Fig. 6. Multifunctional ZapB-GFP-Z IBs decorated with two different antibodies. Representative microscopy images of GFP fluorescence (A), red fluorescence emitted from IgG labeled with Alexa Fluor 555 (B), blue fluorescence emitted from IgG labeled with eFluor 450 (C), and the three images merged (D). (For interpretation of the references to color in this figure legend, the reader is referred to the web version of this article.)

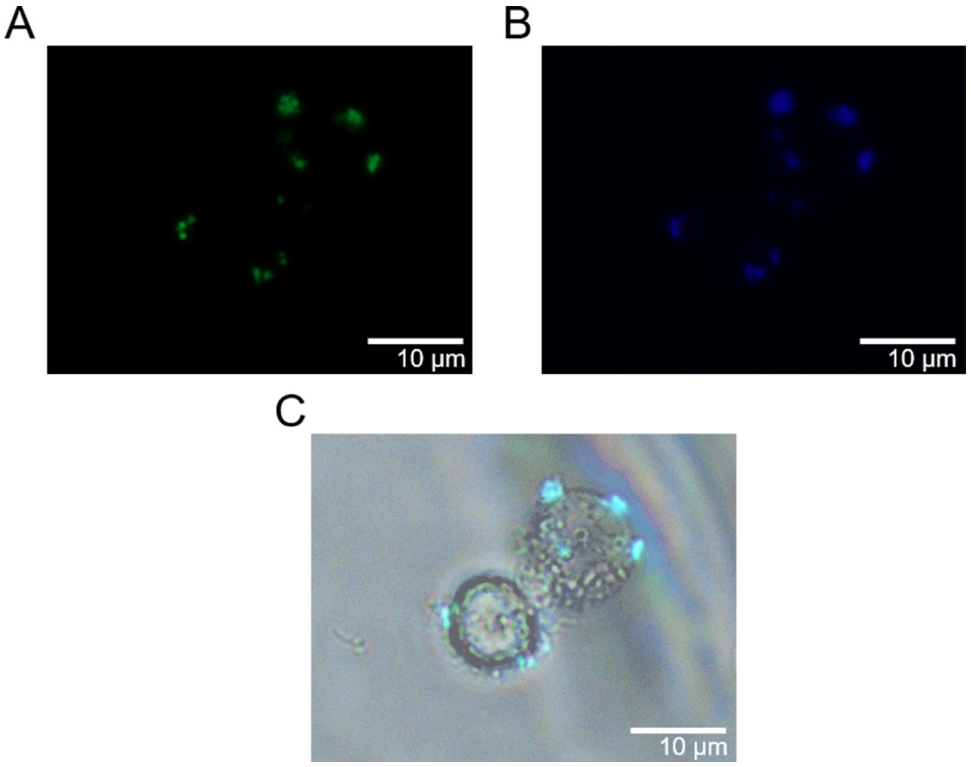

Fig. 7. Specific binding of bifunctional ZapB-GFP-Z IBs to T lymphocytes. Representative microscopy images of GFP fluorescence (A), blue fluorescence emitted from anti-CD3 IgG labeled with eFluor 450 (B), and merging of these images and brightfield image (C). (For interpretation of the references to color in this figure, the reader is referred to the web version of this article.)

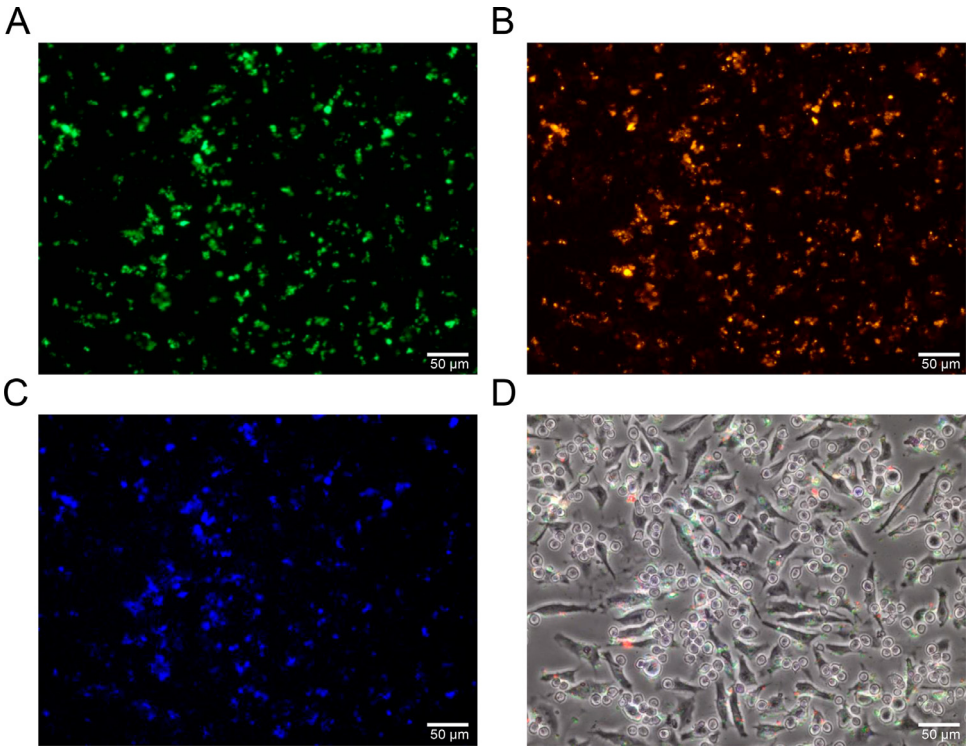

Fig. 8. Dual IgG-decorated ZapB-GFP-Z IBs direct T cells expressing CD3 to HeLa cells expressing EGFR. Representative microscopy images of GFP fluorescence (A), red fluorescence emitted from anti-EGFR IgG labeled with Alexa Fluor 555 (B), blue fluorescence emitted from anti-CD3 IgG labeled with eFluor 450 (C), and merging of these three images and brightfield (D). (For interpretation of the references to color in this figure legend, the reader is referred to the web version of this article.)

Overall, the present proof-of-concept study describes a novel kind of protein-based nanoparticles with potential applications in biomedicine, although the *in vivo* usefulness of this approach needs to be further validated.

5. Conclusion

In this work, we created fluorescent nonamyloid IBs able to capture antibodies with high affinity. These submicrometric, spherical, and α-helix-rich protein nanoparticles are innocuous for human cells. They can potentially recognize any cell type of interest when loaded with the proper antibody. Furthermore, these functional IBs can be easily functionalized by adding different antibodies simultaneously, promoting the association of unrelated cell types, acting as mimics of BsAbs. Their production is cost-effective and fully scalable, and therefore, they are convenient sources of *in vivo* traceable protein nanoparticles for potential biomedical applications.

Funding

This work was funded by the Spanish Ministry of Economy and Competitiveness (BIO2016–78,310-R) and by the Spanish Ministry of Science and Innovation (PID2019–105017RB-I00) to S.V and by ICREA, ICREA-Academia 2015 and 2020 to S.V. M.G.G. was supported by the Spanish Ministry of Science and Innovation via a doctoral grant (FPU16/02465).

Declaration of Competing Interest

The authors declare that they have no competing interests.

Acknowledgments

We are grateful to the UAB Microscopy Service of Barcelona and to Servei de Cultius Cel•lulars, Producció d'Anticossos i Citometria (SCAC) for technical advice. We thank Samuel Peña-Díaz for providing us with purified and aggregated α-synuclein protein. The graphical abstract and Fig. S1 were created with Biorender.com.

Supplementary materials

Supplementary material associated with this article can be found, in the online version, at doi:10.1016/j.actbio.2021.06.040.

References

[1] A. Schrödel, A. De Marco, Characterization of the aggregates formed during recombinant protein expression in bacteria, BMC Biochem. 6 (2005) 1–11, doi:10.1186/1471-2091-6-10.
[2] N. Ferrer-Miralles, J. Domingo-Espín, J. Corchero, E. Vázquez, A. Villaverde, Microbial factories for recombinant pharmaceuticals, Microb. Cell Fact.. 8 (2009) 1–8. 10.1186/1475-2859-8-17.
[3] F. Baneyx, M. Mujacic, Recombinant protein folding and misfolding in Escherichia coli, Nat. Biotechnol. 22 (2004) 1399–1407, doi:10.1038/nbt1029.
[4] U. Rinas, E. Garcia-Fruitós, J.L. Corchero, E. Vázquez, J. Seras-Franzoso, A. Villaverde, Bacterial inclusion bodies: discovering their better half, Trends Biochem. Sci. 42 (2017) 726–737, doi:10.1016/j.tibs.2017.01.005.
[5] A. De Marco, N. Ferrer-Miralles, E. Garcia-Fruitós, A. Mitraki, S. Peternel, U. Rinas, M.A. Trujillo-Roldán, N.A. Valdez-Cruz, E. Vázquez, A. Villaverde, Bacterial inclusion bodies are industrially exploitable amyloids, FEMS Microbiol. Rev. 43 (2019) 53–72, doi:10.1093/femsre/fuy038.
[6] E. García-Fruitós, E. Rodríguez-Carmona, C. Díez-Gil, R.M. Ferraz, E. Vázquez, J.L. Corchero, M. Cano-Sarabia, I. Ratera, N. Ventosa, J. Veciana, A. Villaverde, Surface cell growth engineering assisted by a novel bacterial nanomaterial, Adv. Mater. 21 (2009) 4249–4253, doi:10.1002/adma.200900283.
[7] G. Margreiter, P. Messner, K.D. Caldwell, K. Bayer, Size characterization of inclusion bodies by sedimentation field-flow fractionation, J. Biotechnol. 138 (2008) 67–73, doi:10.1016/j.jbiotec.2008.07.1995.
[8] V.D. Jäger, R. Lamm, K. Küsters, G. Ölçücü, M. Oldiges, K.E. Jaeger, J. Büchs, U. Krauss, Catalytically-active inclusion bodies for biotechnology-General concepts, optimization, and application, Appl. Microbiol. Biotechnol. 104 (2020) 7313–7329, doi:10.1007/s00253-020-10760-3.

[9] A. Villaverde, J.L. Corchero, J. Seras-Franzoso, E. Garcia-Fruitós, Functional protein aggregates: just the tip of the iceberg, Nanomedicine 10 (2015) 2881–2891 (London, England), doi:10.2217/nnm.15.125.
[10] P. Singhvi, A. Saneja, S. Srichandan, A.K. Panda, Bacterial inclusion bodies: a treasure trove of bioactive proteins, Trends Biotechnol. 38 (2020) 474–486, doi:10.1016/j.tibtech.2019.12.011.
[11] R. Kloss, M.H. Limberg, U. Mackfeld, D. Hahn, A. Grünberger, V.D. Jäger, U. Krauss, M. Oldiges, M. Pohl, Catalytically active inclusion bodies of *L*-lysine decarboxylase from *E. coli* for 1,5-diaminopentane production, Sci. Rep. 8 (2018) 1–11, doi:10.1038/s41598-018-24070-2.
[12] U. Krauss, V.D. Jäger, M. Diener, M. Pohl, K.E. Jaeger, Catalytically-active inclusion bodies-carrier-free protein immobilizates for application in biotechnology and biomedicine, J. Biotechnol. 258 (2017) 136–147, doi:10.1016/j.jbiotec.2017.04.033.
[13] V.D. Jäger, R. Lamm, R. Kloß, E. Kaganovitch, A. Grünberger, M. Pohl, J. Büchs, K.E. Jaeger, U. Krauss, A synthetic reaction cascade implemented by colocalization of two proteins within catalytically active inclusion bodies, ACS Synth. Biol. 7 (2018) 2282–2295, doi:10.1021/acssynbio.8b00274.
[14] M. Pesarrodona, T. Jauset, Z.V. Díaz-Riascos, A. Sánchez-Chardi, M.E. Beaulieu, J. Seras-Franzoso, L. Sánchez-García, R. Baltà-Foix, S. Mancilla, Y. Fernández, U. Rinas, S. Schwartz, L. Soucek, A. Villaverde, I. Abasolo, E. Vázquez, Targeting antitumoral proteins to breast cancer by local administration of functional inclusion bodies, Adv. Sci. 6 (2019), doi:10.1002/advs.201900849.
[15] M.V. Céspedes, O. Cano-Garrido, P. Álamo, R. Sala, A. Gallardo, N. Serna, A. Falgàs, E. Voltà-Durán, I. Casanova, A. Sánchez-Chardi, H. López-Laguna, L. Sánchez-García, J.M. Sánchez, U. Unzueta, E. Vázquez, R. Mangues, A. Villaverde, Engineering secretory amyloids for remote and highly selective destruction of metastatic foci, Adv. Mater. 1907348 (2019) 1–9, doi:10.1002/adma.201907348.
[16] S. Ventura, A. Villaverde, Protein quality in bacterial inclusion bodies, Trends Biotechnol. 24 (2006) 179–185, doi:10.1016/j.tibtech.2006.02.007.
[17] M. Carrió, N. González-Montalbán, A. Vera, A. Villaverde, S. Ventura, Amyloid-like properties of bacterial inclusion bodies, J. Mol. Biol. 347 (2005) 1025–1037, doi:10.1016/j.jmb.2005.02.030.
[18] M. Morell, R. Bravo, A. Espargaró, X. Sisquella, F.X. Avilés, X. Fernàndez-Busquets, S. Ventura, Inclusion bodies: specificity in their aggregation process and amyloid-like structure, Biochim. Biophys. Acta-Mol. Cell Res. 1783 (2008) 1815–1825, doi:10.1016/j.bbamcr.2008.06.007.
[19] M. Gil-Garcia, S. Navarro, S. Ventura, Coiled-coil inspired functional inclusion bodies, Microb. Cell Fact. 19 (2020) 1–16, doi:10.1186/s12934-020-01375-4.
[20] V.D. Jäger, R. Kloss, A. Grünberger, S. Seide, D. Hahn, T. Karmainski, M. Piqueray, J. Embruch, S. Longerich, U. Mackfeld, K.E. Jaeger, W. Wiechert, M. Pohl, U. Krauss, Tailoring the properties of (catalytically)-active inclusion bodies, Microb. Cell Fact. 18 (2019) 1–20, doi:10.1186/s12934-019-1081-5.
[21] M. Diener, B. Kopka, M. Pohl, K.E. Jaeger, U. Krauss, Fusion of a coiled-coil domain facilitates the high-level production of catalytically active enzyme inclusion bodies, ChemCatChem 8 (2016) 142–152, doi:10.1002/cctc.201501001.
[22] R. Lamm, V.D. Jäger, B. Heyman, C. Berg, C. Cürten, U. Krauss, K.E. Jaeger, J. Büchs, Detailed small-scale characterization and scale-up of active YFP inclusion body production with Escherichia coli induced by a tetrameric coiled coil domain, J. Biosci. Bioeng. xxx (2020), doi:10.1016/j.jbiosc.2020.02.003.
[23] W. Wang, S. Ventura, Prion domains as a driving force for the assembly of functional nanomaterials, Prion 14 (2020) 170–179, doi:10.1080/19336896.2020.1785659.
[24] R.M. Hoffman, Application of GFP imaging in cancer, Lab. Invest. 95 (2015) 432–452, doi:10.1038/labinvest.2014.154.
[25] M. Tashiro, R. Tejero, D.E. Zimmerman, B. Celda, B. Nilsson, G.T. Montelione, High-resolution solution NMR structure of the *Z* domain of staphylococcal protein A, J. Mol. Biol. 272 (1997) 573–590, doi:10.1006/jmbi.1997.1265.
[26] C. Chen, Q.L. Huang, S.H. Jiang, X. Pan, Z.C. Hua, Immobilized protein ZZ, an affinity tool for immunoglobulin isolation and immunological experimentation, Biotechnol. Appl. Biochem. 45 (2006) 87, doi:10.1042/ba20060055.
[27] W. Choe, T.A. Durgannavar, S.J. Chung, Fc-Binding Ligands of immunoglobulin G: an overview of high affinity proteins and peptides, Materials 9 (2016) (Basel, Switzerland), doi:10.3390/ma9120994.
[28] A. Konrad, A.E. Karlström, S. Hober, Covalent immunoglobulin labeling through a photoactivable synthetic *Z* domain, Bioconjug. Chem. 22 (2011) 2395–2403, doi:10.1021/bc200052h.
[29] M. Ultsch, A. Braisted, H.R. Maun, C. Eigenbrot, 3-2-1: Structural insights from stepwise shrinkage of a three-helix Fc-binding domain to a single helix, Protein Eng. Des.Sel. PEDS 30 (2017) 619–625, doi:10.1093/protein/gzx029.
[30] A.C. Braisted, J.A. Wells, Minimizing a binding domain from protein *A*, PNAS 93 (1996) 5688–5692, doi:10.1073/pnas.93.12.5688.
[31] D. Skokos, J.C. Waite, L. Haber, A. Crawford, A. Hermann, E. Ullman, R. Slim, S. Godin, D. Ajithdoss, X. Ye, B. Wang, Q. Wu, I. Ramos, A. Pawashe, L. Canova, K. Vazzana, P. Ram, E. Herlihy, H. Ahmed, E. Oswald, J. Golubov, P. Poon, L. Havel, D. Chiu, M. Lazo, K. Provoncha, K. Yu, J. Kim, J.J. Warsaw, N.S. Oristian, C.J. Siao, D. Dudgeon, T. Huang, T. Potocky, J. Martin, D. MacDonald, A. Oyejide, A. Rafique, W. Poueymirou, J.R. Kirshner, E. Smith, W. Olson, J. Lin, G. Thurston, M.A. Sleeman, A.J. Murphy, G.D. Yancopoulos, A class of costimulatory CD28-bispecific antibodies that enhance the antitumor activity of CD3-bispecific antibodies, Sci. Trans. Med. 12 (2020), doi:10.1126/scitranslmed.aaw7888.
[32] H. Kantarjian, A. Stein, N. Gökbuget, A.K. Fielding, A.C. Schuh, J.M. Ribera, A. Wei, H. Dombret, R. Foà, R. Bassan, Ö. Arslan, M.A. Sanz, J. Bergeron, F. Demirkan, E. Lech-Maranda, A. Rambaldi, X. Thomas, H.A. Horst, M. Brüggemann, W. Klapper, B.L. Wood, A. Fleishman, D. Nagorsen, C. Holland, Z. Zimmerman, M.S. Topp, Blinatumomab versus chemotherapy for advanced acute Lymphoblastic Leukemia, N. Engl. J. Med. 376 (2017) 836–847, doi:10.1056/NEJMoa1609783.
[33] C. Rader, Bispecific antibodies in cancer immunotherapy, Curr. Opin. Biotechnol. 65 (2020) 9–16, doi:10.1016/j.copbio.2019.11.020.
[34] H. Liu, A. Saxena, S.S. Sidhu, D. Wu, Fc engineering for developing therapeutic bispecific antibodies and novel scaffolds, Front. Immunol. 8 (2017) 1–15, doi:10.3389/fimmu.2017.00038.
[35] A.K. Kosmides, J.W. Sidhom, A. Fraser, C.A. Bessell, J.P. Schneck, Dual targeting nanoparticle stimulates the immune system to inhibit tumor growth, ACS Nano 11 (2017) 5417–5429, doi:10.1021/acsnano.6b08152.
[36] M.C. Lo Giudice, F. Meder, E. Polo, S.S. Thomas, K. Alnahdi, S. Lara, K.A. Dawson, Constructing bifunctional nanoparticles for dual targeting: improved grafting and surface recognition assessment of multiple ligand nanoparticles, Nanoscale 8 (2016) 16969–16975, doi:10.1039/c6nr05478a.
[37] J. Pujols, S. Peña-Díaz, M. Conde-Giménez, F. Pinheiro, S. Navarro, J. Sancho, S. Ventura, High-throughput screening methodology to identify alpha-synuclein aggregation inhibitors, Int. J. Mol. Sci. 18 (2017), doi:10.3390/ijms18030478.
[38] T. Heimburg, J. Schünemann, K. Weber, N. Geisler, FTIR-spectroscopy of multistranded coiled coil proteins, Biochemistry 38 (1999) 12727–12734, doi:10.1021/bi983079h.
[39] R. Sabaté, S. Ventura, Cross-β-sheet supersecondary structure in amyloid folds: techniques for detection and characterization, Methods Mol. Biol. 932 (2013) 237–257, doi:10.1007/978-1-62703-065-6_15.
[40] A. Espargaró, S. Llabrés, S.J. Saupe, C. Curutchet, F.J. Luque, R. Sabaté, On the binding of congo red to amyloid fibrils, Angew. Chem. Int. Ed. Engl. 59 (2020) 8104–8107, doi:10.1002/anie.201916630.
[41] D. Li, F. Chen, J. Ding, N. Lin, Z. Li, X. Wang, Knockdown of HIP1 expression promotes ligand-induced endocytosis of EGFR in HeLa cells, Oncol. Rep. 38 (2017) 3387–3391, doi:10.3892/or.2017.6025.
[42] N. Normanno, A. De Luca, C. Bianco, L. Strizzi, M. Mancino, M.R. Maiello, A. Carotenuto, G. De Feo, F. Caponigro, D.S. Salomon, Epidermal growth factor receptor (EGFR) signaling in cancer, Gene 366 (2006) 2–16, doi:10.1016/j.gene.2005.10.018.
[43] M.S. Kuhns, H.B. Badgandi, Piecing together the family portrait of TCR-CD3 complexes, Immunol. Rev. 250 (2012) 120–143, doi:10.1111/imr.12000.
[44] E. García-Fruitós, E. Vázquez, C. Díez-Gil, J.L. Corchero, J. Seras-Franzoso, I. Ratera, J. Veciana, A. Villaverde, Bacterial inclusion bodies: making gold from waste, Trends Biotechnol. 30 (2012) 65–70, doi:10.1016/j.tibtech.2011.09.003.
[45] S.T.T. Schetters, W.S.P. Jong, L.J.W. Kruijssen, H.B. van den, B. van Saparoea, S. Engels, W.W.J. Unger, D. Houben, J.M.M. den Haan, J. Luirink, Y. van Kooyk, Bacterial inclusion bodies function as vehicles for dendritic cell-mediated *T* cell responses, Cell. Mol. Immunol. 17 (2020) 415–417, doi:10.1038/s41423-019-0298-x.
[46] M.V. Céspedes, Y. Fernández, U. Unzueta, R. Mendoza, J. Seras-Franzoso, A. Sánchez-Chardi, P. Álamo, V. Toledo-Rubio, N. Ferrer-Miralles, E. Vázquez, S. Schwartz, I. Abasolo, J.L. Corchero, R. Mangues, A. Villaverde, Bacterial mimetics of endocrine secretory granules as immobilized *in vivo* depots for functional protein drugs, Sci. Rep. 6 (2016) 1–10, doi:10.1038/srep35765.
[47] R. Kloss, T. Karmainski, V.D. Jäger, D. Hahn, A. Grünberger, M. Baumgart, U. Krauss, K.E. Jaeger, W. Wiechert, M. Pohl, Tailor-made catalytically active inclusion bodies for different applications in biocatalysis, Catal. Sci. Technol. 8 (2018) 5816–5826, doi:10.1039/c8cy01891j.
[48] J. Seras-Franzoso, C. Dez-Gil, E. Vazquez, E. Garca-Fruits, R. Cubarsi, I. Ratera, J. Veciana, A. Villaverde, Bioadhesiveness and efficient mechanotransduction stimuli synergistically provided by bacterial inclusion bodies as scaffolds for tissue engineering, Nanomedicine 7 (2012) 79–93, doi:10.2217/nnm.11.83.
[49] Š. Peternel, R. Komel, Isolation of biologically active nanomaterial (inclusion bodies) from bacterial cells, Microb. Cell Fact. 9 (2010) 1–16, doi:10.1186/1475-2859-9-66.
[50] L. Gifre-Renom, J. Seras-Franzoso, D. Rafael, F. Andrade, O. Cano-Garrido, F. Martinez-Trucharte, E. Ugarte-Berzal, E. Martens, L. Boon, A. Villaverde, G. Opdenakker, S. Schwartz, A. Arís, E. Garcia-Fruitós, The biological potential hidden in inclusion bodies, Pharmaceutics 12 (2020), doi:10.3390/pharmaceutics12020157.
[51] A.F. Labrijn, M.L. Janmaat, J.M. Reichert, P.W.H.I. Parren, Bispecific antibodies: a mechanistic review of the pipeline, Nat. Rev. Drug Discov. 18 (2019) 585–608, doi:10.1038/s41573-019-0028-1.
[52] M. Arruebo, M. Valladares, Á. González-Fernández, Antibody-conjugated nanoparticles for biomedical applications, J. Nanomater. 2009 (2009), doi:10.1155/2009/439389.